Loss function of tumor suppressor FRMD8 confers resistance to tamoxifen therapy via a dual mechanism

Weijie Wu[1#], Miao Yu[1#], Qianchen Li[1], Yiqian Zhao[1], Lei Zhang[1], Yi Sun[1], Zhenbin Wang[1], Yuqing Gong[1], Wenjing Wang[2], Chenying Liu[3], Jing Zhang[1], Yan Tang[1], Xiaojie Xu[4]*, Xiaojing Guo[3]*; Jun Zhan[1]*, Hongquan Zhang[1]*

[1]Program for Cancer and Cell Biology, Department of Human Anatomy, Histology and Embryology, School of Basic Medical Sciences; Peking University International Cancer Institute; and State Key Laboratory of Molecular Oncology, Peking University Health Science Center, Beijing 100191, China.

[2]Department of Gastroenterology, Beijing Friendship Hospital, Capital Medical University; State Key Laboratory for Digestive Health; National Clinical Research Center for Digestive Diseases，Beijing 100050, China.

[3]Department of Breast Pathology and Lab; Tianjin Medical University Cancer Institute & Hospital; National Clinical Research Center for Cancer; Key Laboratory of Breast Cancer Prevention and Therapy of Ministry of Education of China, Tianjin Medical University; Tianjin's Clinical Research Center for Cancer, Tianjin 300060, China.

[4]Department of Genetic Engineering, Beijing Institute of Biotechnology, Beijing 100071, China.

# These two authors contributed equally to this study.

Running title: Loss of FRMD8 downregulates ERα level

Word number of texts: 7,239

Characters with space: 49,894

* Corresponding authors

Hongquan Zhang, Ph.D.; Professor
Peking University Health Science Center,
#38 Xue Yuan Road, Haidian District, Beijing 100191, China.
Tel: 008610-82802424, E-mail: Hongquan.Zhang@bjmu.edu.cn
Or
Jun Zhan, M.D. & Ph.D.; Associate Professor
Peking University Health Science Center,
#38 Xue Yuan Road, Haidian District, Beijing 100191, China.
E-mail: Zhanjun@bjmu.edu.cn

Or
Xiaojing Guo, M.D. & Ph.D.
Tianjin Medical University Cancer Institute & Hospital,
West Huanhu Road, Tianjin 300060, China.
E-mail: guoxiaojing@tjmuch.com
Or
Xiaojie Xu, M.D. & Ph.D.; Associate Professor
Department of Genetic Engineering, Beijing Institute of Biotechnology,
Beijing 100071, China.
E-mail: miraclexxj@126.com

Impact Statement

Tumor suppressive protein FRMD8 inhibits breast cancer progression by regulating the level of ERα and has the possibility to be a potential target for overcoming tamoxifen treatment resistance.

Abstract

Approximately 40% ERα-positive breast cancer patients suffer from therapeutic resistance to tamoxifen. Although reduced ERα level is the major cause of tamoxifen resistance, the underlying mechanisms remain elusive. Here, we report that FRMD8 raises the level of ERα at both transcriptional and post-translational layers. FRMD8 deficiency in *MMTV-Cre*$^{+}$; *Frmd8*$^{fl/fl}$; *PyMT* mice accelerates mammary tumor growth and loss of luminal phenotype, and confers tamoxifen resistance. Single-cell RNA profiling reveals that Frmd8 loss decreases the proportion of hormone-sensing differentiated epithelial cells and downregulates the levels of ERα. Mechanically, on one hand, loss of FRMD8 inhibits *ESR1* transcription via suppressing the expression of FOXO3A, a transcription factor of *ESR1*. On the other hand, FRMD8 interacts both with ERα and UBE3A, and disrupts the interaction of UBE3A with ERα, thereby blocking UBE3A-mediated ERα degradation. In breast cancer patients, *FRMD8* gene promoter is found hypermethylated and low level of FRMD8 predicts poor prognosis. Therefore, FRMD8 is an important regulator of ERα and may control therapeutic sensitivity to tamoxifen in ERα-positive breast cancer patients.

Keywords: FRMD8; Breast cancer; ERα; Tamoxifen resistance; UBE3A

Introduction

Breast cancer is the most commonly diagnosed cancer worldwide(Sung et al., 2021) and more than 70% of breast cancer are estrogen receptor α (ERα)-positive(Habara & Shimada, 2022). Although endocrine therapy is the most common systemic treatment for ERα-positive breast cancer in clinical practice, approximately 40% of patients still develop primary or secondary resistance to endocrine therapy(Badia et al., 2007; Légaré & Basik, 2016; Rondón-Lagos et al., 2016). Therefore, it is urgent and necessary to explore the mechanisms of endocrine therapy resistance and search for new therapeutic targets.

ERα is a ligand-activated transcription factor that is activated by oestrogen, and promotes cell proliferation during breast cancer development (Harbeck et al., 2019). Tamoxifen (TAM), a selective estrogen receptor antagonist, is the most widely used medicine in endocrine therapy. Tamoxifen competes with estrogen to bind with ERα and changes the conformation of ERα, thereby preventing the interaction between co-activators and ERα and inhibiting activation of ERα (Katzenellenbogen et al., 2018). Thus, the level of ERα is strongly correlated with reactivity and resistance of endocrine therapy. Uncovering the mechanisms by which ERα expression is regulated is essential for overcoming endocrine therapy resistance. Multiple transcription factors, such as AP-2γ, FOXO3, FOXM1, and GATA3, have been reported to bind to the promoter region of *ESR1*, the gene encoding ERα, and participate in transcriptional regulation of *ESR1*(Jia et al., 2019; Koš et al., 2001). In addition, post-translational modifications of ERα, including phosphorylation, acetylation, and ubiquitination, also have effects on subcellular localization, transcriptional activity, and stability of ERα(Rogatsky et al., 1999; Williams et al., 2009; Zhou & Slingerland, 2014). However, the mechanisms underlying the regulation of ERα expression are still not clear and require further investigation.

FERM domain-containing proteins are widely involved in processes such as the formation of macromolecular complexes, subcellular localization, functional activation,

and signal transduction, thereby regulating the occurrence and development of tumors(Frame et al., 2010; Moleirinho et al., 2013; Zhan & Zhang, 2018). FRMD8, as a member of FERM domain-containing proteins, has been reported to bind with iRhom and enhance the stability of the iRhom/TACE complex on the cell surface, thereby preventing iRhom/TACE degradation mediated by lysosomes. TACE is responsible for cleaving and releasing TNF, and the absence of FRMD8 impairs the production of TNF(Künzel et al., 2018; Oikonomidi et al., 2018). Additionally, FRMD8 expressions in both microenvironment and tumor cells promote lung tumor growth(Badenes et al., 2023). FRMD8 inhibits colon cancer growth by preventing cell cycle progression. FRMD8 disrupts the interaction of CDK7 with CDK4, subsequently inhibiting CDK4 activation. Furthermore, FRMD8 competes with MDM2 to bind RB, thereby attenuating MDM2-mediated RB degradation(Yu et al., 2023). However, the roles of FRMD8 in breast tumorigenesis and progression need further exploration.

In this study, we found that loss of Frmd8 in luminal epithelial cells of *MMTV-PyMT* mice accelerates mammary tumor progression and luminal epithelial phenotype loss, and confers tamoxifen resistance. Single-cell RNA profiling reveals that the number of hormone-sensing differentiated cells is diminished and the level of ERα is decreased in Frmd8-knocked-out mammary tumors. FRMD8 not only increases *ESR1* expression, but also prevents ERα degradation by interrupting the interaction between ERα and E3 ligase UBE3A. Further, a low FRMD8 level predicts poor prognosis in human breast cancer patients. Thus, we demonstrated that FRMD8 is an important ERα regulator and a vital tumor suppressive protein in breast cancer growth and drug resistance.

Results

Loss of Frmd8 promotes mammary tumor growth and generates tamoxifen resistance *in vivo*

To examine whether FRMD8 plays a role in breast tumorigenesis, we established luminal epithelium-specific *Frmd8* knockout mice (*MMTV-Cre*$^{+}$; *Frmd8*$^{fl/fl}$) (Fig. 1A and 1B) and further generated a Frmd8-deletion breast cancer mouse model (*MMTV-Cre*$^{+}$; *Frmd8*$^{fl/fl}$; *PyMT*) by crossing *MMTV-Cre*$^{+}$; *Frmd8*$^{fl/fl}$ mice with *MMTV-PyMT* (*PyMT*) mice, a widely used transgenic mouse model of mammary tumorigenesis (Fig. 1C, 1D, S1A and S1B). Compared with *MMTV-Cre*$^{-}$; *Frmd8*$^{fl/fl}$; *PyMT* mice, Frmd8 depleted in mice significantly promotes mammary tumor development (Fig. 1E and 1F). The total tumor weight (Fig. 1G) and number of tumors (Fig. 1H) were markedly higher in *MMTV-Cre*$^{+}$; *Frmd8*$^{fl/fl}$; *PyMT* mice than the control mice. Histological examination of the breast tumors from *PyMT* mice using haematoxylin-eosin (H&E) staining revealed that the luminal epithelium was poorly differentiated in *MMTV-Cre*$^{+}$; *Frmd8*$^{fl/fl}$; *PyMT* mice tumors compared with the control mice (Fig. 1I). Furthermore, immunohistochemical staining showed that the percentage of Ki67-positive cells was significantly elevated in mammary tumors of *Frmd8*-depleted mice (Fig. 1J and 1K). Consistently, 5-ethynyl-2'-deoxyuridine (EdU) incorporation assays demonstrated that FRMD8 depletion promoted human breast cancer cell MCF7 and T47D proliferation (Fig. S1C and S1D). These findings indicated that *Frmd8* deficiency in the luminal epithelium accelerates mammary tumor growth in *MMTV-PyMT* mice and promotes cell proliferation.

Since tamoxifen is commonly used for the treatment of ERα^{+}/HER2^{-} breast cancer，we thus investigated whether loss of Frmd8 affects sensitivity of mammary tumors to tamoxifen treatment in mice. To this end, *MMTV-Cre*$^{-}$; *Frmd8*$^{fl/fl}$; *PyMT* mice and *MMTV-Cre*$^{+}$; *Frmd8*$^{fl/fl}$; *PyMT* mice were injected intraperitoneally with tamoxifen or corn oil as control every two days. The results showed that tamoxifen significantly prevents mammary tumor progression in the control mice (Fig. 1L and 1M). However,

mammary tumors of *MMTV-Cre*$^{+}$; *Frmd8*$^{fl/fl}$; *PyMT* mice showed no response to tamoxifen treatment (Fig. 1L and 1M). Consistently, the total tumor weight (Fig. 1N) and number of tumors (Fig. 1O) of *MMTV-Cre*$^{-}$; *Frmd8*$^{fl/fl}$; *PyMT* mice were markedly decreased after tamoxifen treatment, whereas there was no difference in *MMTV-Cre*$^{+}$; *Frmd8*$^{fl/fl}$; *PyMT* mice (Fig. 1N and 1O). Taken together, these findings demonstrated that loss of Frmd8 accelerates mammary tumor growth and generates resistance to tamoxifen therapy in Frmd8-depleted mice.

Frmd8 knockout decreases the proportion of the hormone-sensing differentiated epithelial cells

To investigate the mechanism through which Frmd8 loss promotes mammary tumor growth and leads to tamoxifen resistance, we then performed single-cell RNA sequencing (scRNA-seq) analysis. Mammary tumors from 4-month-old *MMTV-Cre*$^{-}$; *Frmd8*$^{fl/fl}$; *PyMT* and *MMTV-Cre*$^{+}$; *Frmd8*$^{fl/fl}$; *PyMT* mice were harvested and analyzed using the Chromium Single Cell 3' Reagent Kitsv3 (10× Genomics). Cells that passed quality control (QC) filter totaled 24,320, of which 11,606 cells were from *MMTV-Cre*$^{-}$; *Frmd8*$^{fl/fl}$; *PyMT*, and 12,714 cells were from *MMTV -Cre*$^{+}$; *Frmd8*$^{fl/fl}$; *PyMT* mice (Fig. 2A). After that, we profiled the three major cell lineages, including epithelial cells, immune cells and stromal cells by the UMAP visualization (Fig. 2B). Their associated top-expressed and canonical markers were shown in Figure S2A and S2B, respectively. Based on the expression of known markers, a total of 12 clearly separated cell lineages were finally identified (Fig. 2C and 2D). In particular, they were as follows: B cells highly expressing *Cd19*, *Cd79a*, *Cd79b*; CD4^{+} T cells characterized with high *Cd3g* and *Cd4* expression; CD8^{+} T cells highly expressing *Cd3g* and *Cd8a*; dendritic cells (DCs) expressing *Cd74* and *Cd14*； endothelial cells specifically expressing the markers *Pecam1* and *Emcn*; epithelial cells expressing *Epcam* and *Krt8*; fibroblast cells high expressing *Col1a1* and *Col3a1*; granulocyte cells specifically expressing the markers *S100a9*; macrophage cells highly expressing *Cd14*, *Cd68* and *C1qa*; monocyte cells

highly expressing *Cd14* and *Ccr2*; natural killer (NK) cells specifically expressing *Nkg7* and *Ncr1* (Fig. S2C). The dot plots compared the proportion of cells expressing cluster-specific markers and their scaled relative expression levels (Fig. S2D).

To further explore whether the proportions of epithelial cells in mammary tumors were affected by Frmd8 loss, we subset and re-identified four epithelial cell clusters(Valdes-Mora et al., 2021), including alveolar progenitor (Avp), basal (Bsl), hormone-sensing differentiated (Hsd) and luminal progenitor (Lp) epithelial cells (Fig. 2E). As expected, the epithelial cells were composed of luminal epithelial cells and basal epithelial cells, which were consistent with the cellular characteristics of the mammary glands. In contrast to control mice, the proportion of the Hsd epithelial cells was significantly decreased in *MMTV-Cre*$^{+}$; *Frmd8*$^{fl/fl}$; *PyMT* mice (Fig. 2F).

To define the tumor cells in the mouse mammary tumors, we applied inferCNV algorithm to calculate the copy number variations (CNVs) of the single cells (Fig. 2G). To this end, we analyzed CNV scores of epithelial subclusters, immune and stromal cells, revealing immune cells with low CNV score (Fig. 2H). Given that Hsd epithelial cells which specifically expressed *Esr1* and *Pgr* had lower CNV score than alveolar progenitor (Avp), basal (Bsl) and luminal progenitor (Lp) epithelial cells, we defined the low CNV score Hsd epithelial cells as normal cells (Fig. 2H and 2I). Furthermore, we defined the high CNV score epithelial cells as tumor cells, and plotted the UMAP visualization (Fig. 2J). The results also showed that the expression of *Frmd8* was decreased in tumor cells compared with normal cells (Fig. 2K and S2E). In addition, we observed that loss of Frmd8 significantly decreased the expression of *Esr1* and *Pgr* in normal cells of mammary tumors, and decreased expression of Frmd8 in tumor cells accompanied with low expression of *Esr1* and *Pgr* compared with normal cells (Fig. 2L and S2E). Taken together, these findings indicated that Frmd8 depletion in *PyMT* mice leads to decreases of the Hsd epithelial cells proportion and the expression of *Esr1* and *Pgr*.

FRMD8 promotion of *ESR1* expression is mediated by FOXO3A

Given that scRNA-seq results suggested that loss of Frmd8 reduced the proportion of Hsd epithelial cells and the expression of *Esr1* and *Pgr*, multiple immunofluorescence staining analyses were then performed to examine the change of ERα and PR at the protein levels *in situ* in mammary tumors of 4-month-old Frmd8-depleted mice. Consistent with the scRNA-seq results, deficiency of Frmd8 dramatically decreased the levels of ERα, PR and CK8, a marker of mammary luminal epithelium, in normal tissues adjacent to tumors (Fig. 3A and 3B). *In situ* tissue flow cytometry analysis demonstrated that in normal tissues adjacent to tumor of the control mice, the proportion of ERα-positive cells among $CK8^+$ cells were 45.49%, whereas this proportion was just 9.28% in *MMTV-Cre*$^+$; *Frmd8*$^{fl/fl}$; *PyMT* mice (Fig. S3A). Similarly, the proportion of PR-positive cells among $CK8^+$ cells was also reduced in normal tissues adjacent to tumor of *MMTV-Cre*$^+$; *Frmd8*$^{fl/fl}$; *PyMT* mice compared with the control mice (Fig. S3B). FRMD8^{high}ERα^{high} and FRMD8^{high}PR^{high} cells were mainly present in normal tissues adjacent to tumor of *MMTV-Cre*$^-$; *Frmd8*$^{fl/fl}$; *PyMT* mice, whereas Frmd8 depletion led to FRMD8^{low}ERα^{low} and FRMD8^{low}PR^{low} cells markedly increased (Fig. S3C and S3D). In mammary tumor tissues from both control mice and *MMTV-Cre*$^+$; *Frmd8*$^{fl/fl}$; *PyMT* mice, the expressions of ERα and PR were almost negative (Fig. 3A and 3B). Since the expression of ERα is loss with tumor progression, to further clarify the regulation of Frmd8 on ERα, we performed immunohistochemistry (IHC) staining of mammary glands of 7-week-old *PyMT* mice, which had no palpable tumors. The results showed that Frmd8 depletion also markedly decreased the expression of ERα in normal and atypical hyperplasia breast tissues (Fig. S3E). Taken together, these data suggested that deficiency of FRMD8 downregulates the protein levels of ERα and PR in mammary tissues of *MMTV-PyMT* mice, and accelerates the loss of luminal phenotype in mammary gland.

It was known that the common endocrine treatment for non-metastatic breast cancer relies on the expression of ERα(Waks & Winer, 2019) and our results demonstrated that

loss of Frmd8 promotes mammary tumor growth and confers tamoxifen resistance in mice, we thus aim to further examine whether FRMD8 regulates ERα expression. To this end, we transiently transfect Flag-FRMD8 vector or FRMD8 siRNA in human breast cancer cells. Our results showed that FRMD8 overexpression drastically increased the levels of ERα, while ERα expression was greatly downregulated when FRMD8 was knocked down (Fig. 3C and 3D). Moreover, qRT-PCR results indicated that depletion of FRMD8 significantly decreased the mRNA level of *ESR1* (Fig. 3E).

FOXO3A is a crucial transcription factor for ERα(Jia et al., 2019). To answer whether FOXO3A is involved in the regulation of FRMD8 on ERα, we examined the expression of FOXO3A after silencing FRMD8 through transfecting siRNA into MCF7 and T47D cells. The results showed that FRMD8 silencing dramatically decreased the level of FOXO3A (Fig. 3F). Consistently, overexpression of FRMD8 in MCF7 and T47D cells markedly raised the level of FOXO3A (Fig. 3G). To examine whether FRMD8 promotes *ESR1* transcription through FOXO3A, HA-tagged FRMD8 as well as FOXO3A siRNA were co-transfected into MCF7 cells. Although exogenous FRMD8 significantly upregulated ERα expression, depletion of endogenous FOXO3A greatly reduced the effect of FRMD8 on ERα (Fig. 3H and 3I). Besides, chromatin immunoprecipitation (ChIP)-qPCR was performed and revealed that depletion of FRMD8 significantly decreased the occupancy of FOXO3A at the *ESR1* promoters (Fig. 3J). Altogether, these data indicated that FRMD8 promoted upregulation of *ESR1* is mediated by FOXO3A (Fig. 3K).

FRMD8 stabilizes ERα via prevention of its degradation

Although our results suggest that FRMD8 depletion inhibits the mRNA level of *ESR1*, unexpectedly, we also observed that decreased expression of FRMD8 led to a decreased level of exogenous Flag-ERα (Fig. 4A). This result suggested that in addition to inhibiting mRNA expression of ERα, FRMD8 may also regulate ERα protein expression at the post-translational level. To this end, T47D cells were treated with

cycloheximide (CHX), a protein synthesis inhibitor. Depletion of FRMD8 greatly increased the ERα turnover rate and the half-life of ERα decreased from 6 h to approximately 2 h (Fig. 4B and 4C). Furthermore, MCF7 and T47D cells were treated with MG132, a proteasome inhibitor, and chloroquine (CQ), a lysosome inhibitor, to determine whether ERα degradation was mediated by the proteasome or the lysosome. The results showed that the reduction of ERα levels by FRMD8 depletion was blocked by treatment with MG132 but not CQ (Fig 4D). Altogether, these data suggested that FRMD8 stabilizes ERα protein via a proteasome-mediated degradation pathway.

FRMD8 inhibits ERα degradation by blocking UBE3A binding with ERα

Given that FERM domain containing proteins play roles via regulating protein-protein interaction, we wonder whether there is an interaction between FRMD8 and ERα. To this end, co-immunoprecipitation (co-IP) assays were performed using Flag-FRMD8 in MCF7 and T47D cells to examine the association of exogenous FRMD8 with endogenous ERα. The results showed that FRMD8 interacts with ERα (Fig. 5A and 5B). Importantly, an interaction between endogenous FRMD8 and endogenous ERα was also observed in MCF7 cells (Fig. 5C). Furthermore, a glutathione S-transferase (GST) pull-down assay using purified recombinant GST-FRMD8 and Flag-tagged ERα proteins was also performed. The results indicated that FRMD8 interacts directly with ERα *in vitro* (Fig. 5D). Taken together, these findings suggest that FRMD8 is a binding partner of ERα in human cells.

The aforementioned findings demonstrated that FRMD8 prevents ERα degradation via proteasome pathway. To explore the mechanism by which FRMD8 inhibits ERα degradation, co-IP assay and mass spectrometry (MS) analysis were performed in HEK293A cells transiently expressing Flag-FRMD8 (Table S1). We next searched for the FRMD8-interacting proteins identified by MS matched with the known E3 ubiquitin ligases of ERα. Interestingly, UBE3A, a ubiquitin ligase for ERα(Sun et al., 2012), is the only matched protein that interacts with FRMD8 (Fig. 5E). We thus examined the

interaction between FRMD8 and UBE3A through co-IP. The results indicated an interaction between FRMD8 and UBE3A (Fig. 5F and 5G). Further, we assumed that FRMD8 may interfere with the interaction between ERα and UBE3A. To test this idea, co-IP assays were performed in HEK293T and T47D cells. In both cell types, the level of ERα ubiquitination and the interaction between ERα and UBE3A were markedly increased by FRMD8 depletion (Fig. 5H and 5I). Intriguingly, FRMD8 depletion led to a marked decrease of ERα expression, while depletion of UBE3A dramatically rescued the effect of FRMD8 depletion (Fig. 5J and 5K). Taken together, these results strongly demonstrated that FRMD8 binds to ERα and UBE3A, and prevents UBE3A interaction with ERα, thereby blocking UBE3A-mediated ERα ubiquitination and degradation (Fig. 5L).

FRMD8 **promoter is methylated and low FRMD8 level predicts poor prognosis in breast cancer patients**

Given that Frmd8 prevents mammary tumor growth and inhibits tumor cell proliferation in mice (Fig. 1), we would like to investigate whether the expression of FRMD8 is downregulated in mammary tumors. ScRNA-seq results demonstrated that the level of *Frmd8* in normal Hsd epithelial cells was significantly higher than other tumor cells in the mammary tumors from *PyMT* mice (Fig. 6A). To further verify the expression of FRMD8 in human breast cancer cell lines, whole cell lysates from normal mammary epithelial cells and various subtypes of breast cancer cell lines were subjected to Western blot analysis. Results showed that FRMD8 expression was lower in claudin-low breast cancer cell lines compared with normal mammary epithelial cell line or ERα-positive cell lines (Fig. 6B).

Hypermethylation of tumor suppressor genes is one of the major causes for tumorigenesis. Therefore, we investigated whether the promoter region of FRMD8 is hypermethylated in breast cancer patients. An analysis based on TCGA database showed that the *FRMD8* promoter was highly methylated in primary breast tumors (Fig.

6C). Subsequently, breast cancer cells were treated with the DNA methyltransferase inhibitor 5-aza-2-deoxycytidine (5-Aza-dC). The results showed that 5-Aza-dC treatment significantly upregulated both mRNA and protein levels of FRMD8 in claudin-low but not luminal breast cancer cell lines (Fig. 6D, 6E and S4A), which was consistent with the lower expression of FRMD8 in claudin-low breast cancer cell lines (Fig. 6A). These findings demonstrated that *FRMD8* gene promoter is hypermethylated, which could be the reason for the reduced FRMD8 expression in triple-negative breast cancer cells.

To further investigate the clinical significance of FRMD8 in breast cancer patients, we performed immunohistochemical staining of FRMD8 in a tissue microarray of breast cancer patients and evaluated the level of FRMD8 (Fig. 6F). The results suggested that patients with lower level of FRMD8 showed poor overall survival (p=0.0409) (Fig. 6G). Moreover, we also found that a decreased FRMD8 level was associated with poor recurrence free survival in breast cancer patients according to Kaplan-Meier Plotter analysis (Fig. 6H, 6J, S4B and S4C). Collectively, these data indicated that the promoter of *FRMD8* is hypermethylated, and the low FRMD8 level predicts poor prognosis of breast cancer patients.

Discussion

In this study, we found that FRMD8 plays a tumor suppressive role in breast cancer progression. We demonstrated that loss of FRMD8 promotes mammary tumor growth, accelerates the loss of mammary luminal phenotype, and confers tamoxifen resistance via downregulating ERα level. FRMD8 depletion not only suppresses transcription of *ESR1* through decreasing the level of FOXO3A, but also promotes the E3 ligase UBE3A binding with ERα to disrupts ERα protein stability. Moreover, the promoter of *FRMD8* is hypermethylated and a decreased FRMD8 level predicts poor outcomes in breast cancer patients (Fig. 7).

As a FERM-domain containing protein, FRMD8 is necessary for releasing of TNF

and EGFR ligands(Künzel et al., 2018; Oikonomidi et al., 2018). FRMD8 regulates lung cancer cell growth by regulating tumor microenvironment(Badenes et al., 2023). Frmd8-deficient mice are defective in intestinal epithelial barrier repair function and deletion of Frmd8 promotes colorectal tumorigenesis induced by azoxymethane/ dextran sodium sulfate in mice(Badenes et al., 2023; Yu et al., 2023). FRMD8 acts as a scaffold protein, inhibiting CDK4 activation mediated by CDK7 and preventing MDM2-mediated RB degradation(Yu et al., 2023). In this study, our results suggested that FRMD8 inhibits mammary tumor progression in *MMTV-PyMT* mice. Besides, FRMD8 also acts as a scaffold molecule, which interacts simultaneously with ERα and UBE3A, and renders UBE3A unable to bind with ERα, thus stabilizing ERα.

In *MMTV-PyMT* mice, early-stage mammary tumors express ERα and PR, but these receptors are gradually lost as the tumor progresses (Lapidus et al., 1998). Our scRNA-seq results revealed that mammary tumor epithelial cells in *MMTV-PyMT* mice fall into four clusters, with only Hsd epithelial cells showing ERα and PR expression. Additionally, Hsd epithelial cells exhibited the lowest CNV score, indicating a closer resemblance to normal epithelial cells. The loss of Frmd8 reduced the proportion of Hsd epithelial cells and led to a downregulation of ERα and PR expression, implying that Frmd8 deficiency promotes the loss of luminal features in the mammary gland and accelerates mammary tumor progression.

In this study, we identified that loss of FRMD8 inhibiting *ESR1* expression through downregulating the level of FOXO3A. FOXO3A locates in nucleus and blocks cell cycle progression via activating the cell cycle blocking protein $p27^{KIP1}$ (Seoane et al., 2004). In addition, FOXO3A contributes to cell death through a Fas ligand-dependent mechanism(Seoane et al., 2004). Phosphorylated FOXO3A mediated by AKT binds to 14-3-3 protein and remains in the cytoplasm, resulting in loss of activity(Arden, 2004). Thus, FRMD8 may also be involved in the regulation of cell cycle or apoptosis in an ERα-independent manner by regulating FOXO3A. Furthermore, FOXO3A is closely associated with the stemness of breast cancer cells. FOXO3A suppresses breast cancer

stem cell properties and tumorigenicity via inhibition of FOXM1/SOX2 signaling(Liu et al., 2020; Yan et al., 2017), suggesting that FRMD8 may have an effect on breast cancer stem cells. However, the mechanisms by which FRMD8 promotes FOXO3A expression remain unclear and need to be further investigated.

The proportion of luminal subtype is increasing in new cases of breast cancer(Waks & Winer, 2019). Tamoxifen therapy is one of the most important systemic treatment for $ER\alpha^{+}/HER2^{-}$ subtype breast cancer patients(Waks & Winer, 2019). Unfortunately, primary or secondary tamoxifen resistance occurs in about 40% of patients treated with tamoxifen therapy, and tamoxifen resistance often leads to the development of resistance to other selective estrogen receptor modulators(Badia et al., 2007; Légaré & Basik, 2016; Rondón-Lagos et al., 2016). As a regulator of ERα, FRMD8 may be a therapeutic target for rescue tamoxifen resistance.

In summary, we identified FRMD8 as a prognostic marker in breast cancer. FRMD8 regulates ERα level through a dual mechanism. Loss of FRMD8 inhibits *ESR1* transcription via downregulating FOXO3A expression. FRMD8 also stabilizes ERα protein by preventing UBE3A from binding to ERα. Deficiency of FRMD8 promotes mammary luminal features loss and confers tamoxifen resistance. Our findings indicated that targeting *FRMD8* promoter methylation may provide a novel therapeutic approach for reversing tamoxifen resistance.

Materials and Methods

Mice

Both *Frmd8* floxed mice and *MMTV-PyMT* mice were purchased from Shanghai Model Organisms Center Inc (SMOC). *MMTV-Cre*$^{+}$ mice were from the Nanjing Biomedical Research Institute of Nanjing University.

Frmd8 floxed (*Frmd8*$^{fl/fl}$) mice were crossed with *MMTV-Cre*$^{+}$; *PyMT* transgenic mice to generate *Frmd8* heterozygous (*MMTV-Cre*$^{+}$; *Frmd8*$^{fl/wt}$; *PyMT*) mice. *MMTV-Cre*$^{+}$; *Frmd8*$^{fl/wt}$; *PyMT* mice were further backcrossed with *Frmd8*$^{fl/fl}$ mice to obtain littermate *MMTV-Cre*$^{-}$; *Frmd8*$^{fl/fl}$; *PyMT* and *MMTV-Cre*$^{+}$; *Frmd8*$^{fl/fl}$; *PyMT* mice.

Mice were housed in a pathogen-free animal facility at Laboratory Animal Center of Peking University Health Science Center with a 12 h light/dark cycle, constant temperature and humidity, and fed standard rodent chow and water ad libitum. All animal experiments were approved by the Peking University Biomedical Ethics Committee and the approval number is BCJB0104. Genomic DNA extracted from mouse tail biopsies was subjected to standard genotyping PCR using the primers specified in Table S3. The reaction conditions were: 5 minutes at 94℃; 35 cycles of 30 s at 94℃, 30 s at 56℃ and 1 minute at 72℃; followed by 5 minutes at 72℃ and hold at 4℃.

Tamoxifen treatment

7-week-old female mice were given intraperitoneal injections of either corn oil or tamoxifen (50 mg/kg) every two days. Tumor formation was assessed every two days, and the time point at which the tumor first became palpable was recorded as the tumor-free survival time. At the end of the treatment, mice were euthanized and the total number of tumors were counted. Tumors were measured using calipers, and tumor volume was calculated using the formula: V = (length × width × height × 0.5) mm^3. Tumors were subsequently fixed in 4% paraformaldehyde (PFA) and housed in individual cassettes for paraffin embedding. 5 μm sections were stained for

hematoxylin-eosin (H&E) or immunohistochemistry.

Antibodies and reagents

Antibodies against ERα (#8644), Ubiquitin (#3936) and PR (#8757) were purchased from Cell Signaling Technology. Antibodies specific for ERα (#ab32063), CK8 (#ab53280), FOXO3A (#ab109629), UBE3A (#ab272168) and HER2 (#ab134182) were from Abcam. Anti-PR (#YM3348) antibody was from Immunoway. Anti-FRMD8 (#HPA002861) antibody was from Atlas Antibodies. Anti-Flag (#F3165) antibody was from Sigma-Aldrich. Antibodies against GAPDH (#AC002) was purchased from ABclonal Technology. Anti-Actin (#sc-58673) antibodies was from Santa Cruz Biotechnology. Antibodies specific for β-tubulin (#TA-10) was from Zhong Shan Jin Qiao (ZSGB-Bio).

MG132 (#S2619) was purchased from Selleck. Chloroquine (CQ, #C6628), cycloheximide (#C7698) and 5-aza-2-deoxycytidine (5-Aza-dC; #A3656) were purchased from Sigma-Aldrich. Tamoxifen (#HY-13757A) and estradiol (E2, #HY-B0141) were purchased from MedChemExpress.

Plasmids

The recombinant vectors encoding human FRMD8 and ERα were constructed by PCR-based amplification, and then subcloned into the p3×Flag-CMV^{TM}-10 expression vector. The GST-tagged FRMD8 expression plasmid was generated by inserting PCR-amplified fragments into pGEX-4T-1 vector. All constructs were confirmed by DNA sequencing.

Cell culture

Human embryonic kidney cell lines HEK293T and HEK293A and human breast cancer cell lines MCF7, BT-20, MDA-MB-231 and SUM159 were cultured in Dulbecco's Modified Eagle Medium (DMEM). Human breast cancer cell lines T47D and BT-549

were cultured in RPMI 1640 medium. All media were supplemented with 10% fetal bovine serum, 100 U/ml penicillin and 0.1 mg/ml streptomycin. Medium for culturing T47D was supplemented with 0.2 U/ml insulin. Human breast cancer cell line MCF10A was cultured in DMEM/F12 medium supplemented with 10% horse serum, 100 U/ml penicillin and 0.1 mg/ml streptomycin, 20 ng/ml epidermal growth factor, 0.5 μg/ml hydrocortisone, 10 μg/ml insulin and 100 ng/ml cholera toxin. All cell lines were maintained in a humidified atmosphere at 37°C with 5% CO_2 and passaged using 0.25% trypsin containing 0.02% EDTA for dissociation at 80% confluence.

Plasmid and specific siRNA transfection

For transient transfection, cells at 50%-60% confluence were transfected with plasmids via polyethylenimine (PEI; Polyscience, #24765). For RNA interference experiments, cells at 60-70% confluence were transfected with siRNA using Lipo8000 (Beyotime, # C0533). The specific sequences of siRNA are listed in Table S2.

Extraction of proteins and immunoblotting

Cells or tissues were lysed using RIPA buffer (1×PBS, pH 7.4, 0.5% sodium deoxycholate, 1% NP-40, and 0.1% SDS) complemented with an EDTA-free cocktail of protease inhibitors (Roche). This was followed by centrifugation at 12,000 rpm for over 15 minutes at a temperature of 4°C to collect the supernatant. Protein concentrations were ascertained using a bicinchoninic acid (BCA) protein assay kit (Applygen, #P1511). Protein samples underwent electrophoresis via SDS-PAGE and were then transferred to a polyvinylidene fluoride (PVDF) membrane employing conventional methods. The membranes were treated with 5% non-fat milk for one hour, then incubated with primary antibodies at 4℃ overnight, and subsequently exposed to HRP-conjugated goat anti-mouse or rabbit IgG secondary antibodies for one hour at 4℃. The bound antibodies were visualized using the EZ-ECL Chemiluminescence Detection Kit for HRP (Biological Industries, # 20-500-1000) through

ChampChemiTM (SageCreation).

Chromatin immunoprecipitation

The chromatin immunoprecipitation (ChIP) assay was performed according to the manufacturer's instructions of Sonication ChIP Kit (ABclonal, #RK20258). The purified DNA was analyzed by quantitative reverse transcription PCR (qRT-PCR). All primers are shown in Table S2.

Immunoprecipitation

IgG, serving as controls, or indicated antibodies were added to pre-cleared lysates and allowed to incubate overnight at 4°C with sustained rocking. Following this, lysates were subjected to a 4-hour incubation with 35-50 μl of either protein A or protein G Sepharose beads (Santa Cruz Biotechnology) at 4°C. Subsequently, the Sepharose beads were washed thrice with RIPA buffer and heated in SDS-loading buffer at 99°C for 10 minutes. The immunoprecipitation results were assessed via immunoblotting.

Mass spectrometry analysis

Flag-FRMD8 and empty vector were transiently transfected in HEK293A cells using PEI, and cell lysates were harvested after 48 h. The cell lysates were pre-cleared and then incubated with pre-washed anti-Flag M2 agarose beads (Yeasen, #20584ES08) overnight at 4°C. Beads were washed three times with PBS. Protein samples were then eluted by boiling with sodium dodecyl sulfate (SDS)-loading buffer at 99°C for 10 min. Ten percent of the samples were saved for immunoblotting. The other 90% of samples were separated by SDS-PAGE, visualized by colloidal coomassie blue staining, destained and subjected to mass spectrometry (MS) analysis.

For MS analysis, the protein in the gel was subjected to trypsin digestion. In the LC-MS/MS analysis, the digested products were separated using a 120-minute gradient elution at a flow rate of 0.300 μL/min, utilizing the Thermo Ultimate 3000 nano-UPLC

system directly interfaced with the Thermo Fusion LUMOS mass spectrometer. The analytical column used was an Acclaim PepMap RSLC (75 µm ID, 250 mm length, C18). Mobile phase A consisted of 0.1% formic acid, while mobile phase B was 100% acetonitrile with 0.1% formic acid. The Fusion LUMOS mass spectrometer operated in data-dependent acquisition mode, employing Xcalibur 4.1.50 software. It started with a single full-scan mass spectrum in the Orbitrap (375-1500 m/z, 60,000 resolution), followed by data-dependent MS/MS scans. The MS/MS spectra from each LC-MS/MS run were analyzed against the selected database using Proteome Discovery software (version 2.4).

Recombinant protein expression and GST pull-down assay

For the expression of Glutathione S-transferase (GST) fusion proteins, GST-tagged recombinant vectors were transfected into *Escherichia coli* Rosetta (DE3) cells. Upon the cell culture attaining an OD_{600} between 0.6 and 0.8, the cells were subjected to overnight incubation with 1 mM isopropyl-β-D-thiogalactopyranoside (IPTG; Sigma, #92320) at 20℃. For the purification of GST fusion proteins, cells were collected and sonicated.

For GST-pull down assays, HEK293T cells were transfected and subsequently lysed on ice for over 15 minutes. Purified GST or GST fusion proteins were anchored onto Glutathione Sepharose 4B beads (Pharmacia Biotech). These beads were then further incubated with cellular extract at 4℃ for an extended period of over 4 hours, followed by washes with ice-cold PBS for three times. The process concluded with Western blot analysis.

RNA extraction and qRT-PCR

Total RNA was isolated using Trizol reagent (Invitrogen) as per the manufacturer's guidelines. 1 µg of the isolated RNA was converted to cDNA using HiScript II Q RT SuperMix for qPCR (+gDNA wiper) (Vazyme). Quantitative real-time PCR, carried out

in triplicate, was used to assess relative mRNA levels and was standardized to *GAPDH* expression. The cDNA products were amplified using the LightCycler 96 (Roche) platform, and data were subsequently analyzed through LightCycler 96 (Roche) along with GraphPad Prism 7.0 software. All relevant primers are listed in Table S2.

Histology and immunohistochemistry staining

Tissues were preserved in 4% paraformaldehyde, embedded in paraffin, and then sliced into 5 μm sections prior to staining. Following deparaffinization and rehydration, these sections were subject to H&E staining for structural examination. Immunohistochemistry staining was executed using the streptavidin-biotin-peroxidase complex method, with subsequent detection of 3'3'-diaminobenzidine (DAB) as guided by the manufacturer's instructions (Dako, Agilent pathology solutions). Observations and imaging were performed using an Olympus BX51 microscope coupled with an Olympus DP73 CCD photography system.

Tumor tissue microarray (TMA) immunohistochemistry analysis

Human breast carcinoma TMA (HBre-Duc140Sur-01) was purchased from Shanghai Biochip. Immunohistochemistry staining for FRMD8 in TMA was performed as described above. The stained microarrays were evaluated by a pathologist blind to cancer outcomes. Based on histological evaluations, staining reactivity was categorized into four levels: absence of reactivity (score=0), weak reactivity (score=1), moderate reactivity (score=2), and intense reactivity (score=3 or 4).

Multiple immunohistochemistry staining and analysis

Multicolor immunohistochemistry was conducted using the TissueGnostics Multiple IHC Assay Kit (TissueGnostics, TGFP550) on mammary tumors from mice. Tumors were preserved in 4% paraformaldehyde, embedded in paraffin, and then sliced into 5 μm sections prior to staining. The sections were then deparaffinized and hydrated,

564 followed by antigen retrieval in a Tris-EDTA buffer via microwave. Slides underwent
565 treatment with 3% H_2O_2 at ambient temperature to eliminate endogenous peroxidase
566 activity. For iterative rounds of cyclic staining, slides were treated with blocking
567 solution, then incubated with the primary antibody either overnight at 4℃ or for 2 hours
568 at 37℃, and subsequently with HRP-linked secondary antibody at 37℃ for 30 minutes.
569 Signal was enhanced using Tyramide Signal Amplification (TSA) reagents. Antigen
570 retrieval buffer was applied once more, and the aforementioned steps were repeated for
571 additional staining. Lastly, DAPI was used for 10 minutes to stain nuclei. Tissue images
572 were captured using the tissue faxs platform (TissueGnostics).
573 Immunofluorescence image quantification was carried out via StrataQuest v7.0.158
574 software (TissueGnostics). Cells were identified based on DAPI staining, and the
575 expression levels of Frmd8, ERα, PR, and CK8 were calculated by the software,
576 measuring fluorescence intensity and area to enumerate positively-stained cells. The
577 threshold for identifying positive cells was set by inspecting cell recognition on the
578 original image using the View Backward Data function.
579
580 **EdU (5-ethynyl-2'-deoxyuridine) incorporation assay**
581 The EdU incorporation assay was performed according to the manufacturer's
582 instructions of BeyoClick™ EdU Cell Proliferation Kit with Alexa Fluor 488
583 (Beyotime Biotechnology, #C0071) for cell proliferation.
584
585 **Single-cell RNA sequence (scRNA-seq)**
586 Single-cell RNA sequencing libraries were meticulously prepared utilizing the
587 Chromium Single Cell 3' Reagent Kits v3 according to the protocols recommended by
588 10× Genomics. Briefly, an initial quantity of approximately 1×10^5 cells, which had
589 been sorted through fluorescence-activated cell sorting (FACS), underwent a triple
590 wash process in DPBS containing 0.04% BSA. These cells were subsequently
591 resuspended to a final concentration of 700 to 1,200 cells/μl, with a minimum viability

threshold of 85%. During the library preparation process, cells were encapsulated within droplets to facilitate a precise targeted recovery rate. After the reverse transcription phase, the generated emulsions were disrupted, and the barcoded cDNA was isolated using Dynabeads technology. This was followed by PCR amplification to enrich the cDNA pool. The amplified cDNA served as the template for constructing the 3' gene expression libraries. Specifically, for this construction phase, 50 ng of the amplified cDNA was fragmented and subjected to end repair. This material was then subjected to a double-size selection process using SPRIselect beads. The prepared libraries were sequenced on NovaSeq system provided by Illumina, generating 150 bp paired-end reads.

Single-cell RNA sequence original data process

Prior to commencing the analysis, cellular data underwent a stringent filtering process. Cells with unique molecular identifier (UMI) counts below 30,000 and those exhibiting gene counts within the range of 200 to 5,000 were excluded. Additionally, cells displaying a mitochondrial content exceeding 20% were also removed from further analysis. Following this preprocessing step, the Seurat package (version 2.3) was employed for both dimensionality reduction and cluster identification. The normalization and scaling of gene expression data were accomplished using the NormalizeData and ScaleData functions, respectively. Subsequently, the FindVariableFeatures function facilitated the selection of the 2,000 genes demonstrating the most significant variation for principal component analysis (PCA). Cluster identification was achieved through the FindClusters function, which partitioned the genes into distinct groups. To mitigate batch effects across samples, the Harmony package was utilized. The refined dataset was then visualized in a two-dimensional space employing Uniform Manifold Approximation and Projection (UMAP) techniques, thereby providing insightful representations of the underlying cellular heterogeneity.

Chromosomal copy-number variations estimation

The estimation of chromosomal copy-number variations (CNVs) was conducted utilizing the 'inferCNV' R package. A diverse reference panel comprised of B cells, T cells, NK cells, macrophages and other immune cells facilitated this analysis. Quantification of CNV scores for each subcluster was achieved by aggregating the CNV levels observed across the constituent cells.

Quantification and statistical analysis

Statistical comparisons were performed using unpaired two-tailed Student's t tests, Mann Whitney test, one-way ANOVA or two-way ANOVA. Statistical analyses were performed using GraphPad Prism 9.0 software (GraphPad Software, La Jolla, CA, USA). Data are presented as mean ± the standard error of the mean (SEM). Statistical significance was defined as $p<0.05$.

Data Availability

The accession number for the scRNA-seq data reported in this paper is Gene Expression Omnibus (GEO): GSE244582.

Conflict of Interest Statement

The authors have no potential conflicts of interest.

Acknowledgments

This study was supported by grants from the Ministry of Science and Technology of China 2022YFA1104003 and 2021YFC2501000; National Natural Science Foundation of China grants 82172972, 82230094, 81972616, 81972609 and 81772840; Peking University Medicine Sailing Program for Young Scholars' Scientific & Technological Innovation BMU2024YFJHPY004; the Fundamental Research Funds for the Central Universities; Postdoctoral Fellowship Program of CPSF GZC20230159. We would like to thank TissueGnostics Aisa Pacific Limited for their technical support on multiple immunohistochemistry staining.

Corresponding Authors

Correspondence to Hongquan Zhang or Jun Zhan.

References

Arden, K. C. (2004). FoxO: linking new signaling pathways. *Mol Cell*, *14*(4), 416-418. https://doi.org/10.1016/s1097-2765(04)00213-8

Badenes, M., Burbridge, E., Oikonomidi, I., Amin, A., de Carvalho, É., Kosack, L., Mariano, C., Domingos, P., Faísca, P., & Adrain, C. (2023). The ADAM17 sheddase complex regulator iTAP/Frmd8 modulates inflammation and tumor growth. *Life Science Alliance*, *6*(4). https://doi.org/10.26508/lsa.202201644

Badia, E., Oliva, J., Balaguer, P., & Cavaillès, V. (2007). Tamoxifen resistance and epigenetic modifications in breast cancer cell lines [Review]. *Current Medicinal Chemistry*, *14*(28), 3035-3043. https://doi.org/10.2174/092986707782794023

Frame, M. C., Patel, H., Serrels, B., Lietha, D., & Eck, M. J. (2010). The FERM domain: organizing the structure and function of FAK. *Nat Rev Mol Cell Biol*, *11*(11), 802-814. https://doi.org/10.1038/nrm2996

Habara, M., & Shimada, M. (2022). Estrogen receptor alpha revised: Expression, structure, function, and stability. *Bioessays*, *44*(12), e2200148. https://doi.org/10.1002/bies.202200148

Harbeck, N., Penault-Llorca, F., Cortes, J., Gnant, M., Houssami, N., Poortmans, P., Ruddy, K., Tsang, J., & Cardoso, F. (2019). Breast cancer. *Nat Rev Dis Primers*, *5*(1), 66. https://doi.org/10.1038/s41572-019-0111-2

Jia, X., Li, C., Li, L., Liu, X., Zhou, L., Zhang, W., Ni, S., Lu, Y., Chen, L., Jeong, L. S., Yu, J., Zhang, Y., Zhang, J., He, S., Hu, X., Sun, H., Yu, K., Liu, G., Zhao, H.,…Shao, Z. M. (2019). Neddylation Inactivation Facilitates FOXO3a Nuclear Export to Suppress Estrogen Receptor Transcription and Improve Fulvestrant Sensitivity. *Clin Cancer Res*, *25*(12), 3658-3672. https://doi.org/10.1158/1078-0432.Ccr-18-2434

Katzenellenbogen, J. A., Mayne, C. G., Katzenellenbogen, B. S., Greene, G. L., & Chandarlapaty, S. (2018). Structural underpinnings of oestrogen receptor mutations in endocrine therapy resistance. *Nature Reviews Cancer*, *18*(6), 377-388. https://doi.org/10.1038/s41568-018-0001-z

Koš, M., Reid, G., Denger, S., & Gannon, F. (2001). Minireview: Genomic Organization of the Human ERα Gene Promoter Region. *Molecular Endocrinology*, *15*(12), 2057-2063. https://doi.org/10.1210/mend.15.12.0731

Künzel, U., Grieve, A. G., Meng, Y., Sieber, B., Cowley, S. A., & Freeman, M. (2018). FRMD8 promotes inflammatory and growth factor signalling by stabilising the iRhom/ADAM17 sheddase complex. *eLife*, *7*, e35012. https://doi.org/10.7554/eLife.35012

Lapidus, R. G., Nass, S. J., & Davidson, N. E. (1998). The loss of estrogen and progesterone receptor gene expression in human breast cancer. *J Mammary Gland Biol Neoplasia*, *3*(1), 85-94. https://doi.org/10.1023/a:1018778403001

Légaré, S., & Basik, M. (2016). Minireview: The link between ERα corepressors and histone deacetylases in tamoxifen resistance in breast cancer [Review]. *Molecular Endocrinology*, *30*(9), 965-976. https://doi.org/10.1210/me.2016-1072

Liu, H., Song, Y., Qiu, H., Liu, Y., Luo, K., Yi, Y., Jiang, G., Lu, M., Zhang, Z., Yin, J., Zeng, S., Chen, X., Deng, M., Jia, X., Gu, Y., Chen, D., Zheng, G., & He, Z. (2020). Downregulation of FOXO3a by DNMT1 promotes breast cancer stem cell properties and tumorigenesis. *Cell Death & Differentiation*, *27*(3), 966-983. https://doi.org/10.1038/s41418-019-0389-3

Moleirinho, S., Tilston-Lunel, A., Angus, L., Gunn-Moore, F., & Reynolds, P. A. (2013). The expanding family of FERM proteins. *Biochem J*, *452*(2), 183-193. https://doi.org/10.1042/BJ20121642

Oikonomidi, I., Burbridge, E., Cavadas, M., Sullivan, G., Collis, B., Naegele, H., Clancy, D., Brezinova, J., Hu, T., Bileck, A., Gerner, C., Bolado, A., von Kriegsheim, A., Martin, S. J., Steinberg, F., Strisovsky, K., & Adrain, C. (2018). iTAP, a novel iRhom interactor, controls TNF secretion by policing the stability of iRhom/TACE. *eLife*, *7*, e35032. https://doi.org/10.7554/eLife.35032

Rogatsky, I., Trowbridge, J. M., & Garabedian, M. J. (1999). Potentiation of Human Estrogen Receptor α Transcriptional Activation through Phosphorylation of Serines 104 and 106 by the Cyclin A-CDK2 Complex*. *Journal of Biological Chemistry*, *274*(32), 22296-22302. https://doi.org/https://doi.org/10.1074/jbc.274.32.22296

Rondón-Lagos, M., Villegas, V. E., Rangel, N., Sánchez, M. C., & Zaphiropoulos, P. G. (2016). Tamoxifen resistance: Emerging molecular targets [Review]. *International Journal of Molecular Sciences*, *17*(8), Article 1357. https://doi.org/10.3390/ijms17081357

Seoane, J., Le, H.-V., Shen, L., Anderson, S. A., & Massagué, J. (2004). Integration of Smad and Forkhead Pathways in the Control of Neuroepithelial and Glioblastoma Cell Proliferation. *Cell*, *117*(2), 211-223. https://doi.org/https://doi.org/10.1016/S0092-8674(04)00298-3

Sun, J., Zhou, W., Kaliappan, K., Nawaz, Z., & Slingerland, J. M. (2012). ERα phosphorylation at Y537 by Src triggers E6-AP-ERα binding, ERα ubiquitylation, promoter occupancy, and target gene expression. *Mol Endocrinol*, *26*(9), 1567-1577. https://doi.org/10.1210/me.2012-1140

Sung, H., Ferlay, J., Siegel, R. L., Laversanne, M., Soerjomataram, I., Jemal, A., & Bray, F. (2021). Global Cancer Statistics 2020: GLOBOCAN Estimates of Incidence and Mortality Worldwide for 36 Cancers in 185 Countries. *CA: A Cancer Journal for Clinicians*, *71*(3), 209-249. https://doi.org/https://doi.org/10.3322/caac.21660

Valdes-Mora, F., Salomon, R., Gloss, B. S., Law, A. M. K., Venhuizen, J., Castillo, L., Murphy, K. J., Magenau, A., Papanicolaou, M., Rodriguez de la Fuente, L., Roden, D. L., Colino-Sanguino, Y., Kikhtyak, Z., Farbehi, N., Conway, J. R. W., Sikta, N., Oakes, S. R., Cox, T. R., O'Donoghue, S. I.,…Gallego-Ortega, D. (2021). Single-cell transcriptomics reveals involution mimicry during the specification of the basal breast cancer subtype. *Cell Rep*, *35*(2), 108945. https://doi.org/10.1016/j.celrep.2021.108945

Waks, A. G., & Winer, E. P. (2019). Breast Cancer Treatment: A Review. *Jama*, *321*(3), 288-300. https://doi.org/10.1001/jama.2018.19323

Williams, C. C., Basu, A., El-Gharbawy, A., Carrier, L. M., Smith, C. L., & Rowan,

B. G. (2009). Identification of four novel phosphorylation sites in estrogen receptor α: impact on receptor-dependent gene expression and phosphorylation by protein kinase CK2. *BMC Biochemistry*, *10*(1), 36. https://doi.org/10.1186/1471-2091-10-36

Yan, H., Li, Q., Wu, J., Hu, W., Jiang, J., Shi, L., Yang, X., Zhu, D., Ji, M., & Wu, C. (2017). MiR-629 promotes human pancreatic cancer progression by targeting FOXO3. *Cell Death & Disease*, *8*(10), e3154-e3154. https://doi.org/10.1038/cddis.2017.525

Yu, M., Wu, W. J., Sun, Y., Yan, H. Y., Zhang, L., Wang, Z. B., Gong, Y. Q., Wang, T. Z., Li, Q. C., Song, J. G., Wang, M. Y., Zhang, J., Tang, Y., Zhan, J., & Zhang, H. Q. (2023). FRMD8 targets both CDK4 activation and RB degradation to suppress colon cancer growth. *Cell Reports*, *42*(8), 112886. https://doi.org/ARTN 112886 10.1016/j.celrep.2023.112886

Zhan, J., & Zhang, H. (2018). Kindlins: Roles in development and cancer progression. *Int J Biochem Cell Biol*, *98*, 93-103. https://doi.org/10.1016/j.biocel.2018.03.008

Zhou, W., & Slingerland, J. M. (2014). Links between oestrogen receptor activation and proteolysis: relevance to hormone-regulated cancer therapy. *Nature Reviews Cancer*, *14*(1), 26-38. https://doi.org/10.1038/nrc3622

Figure Legends

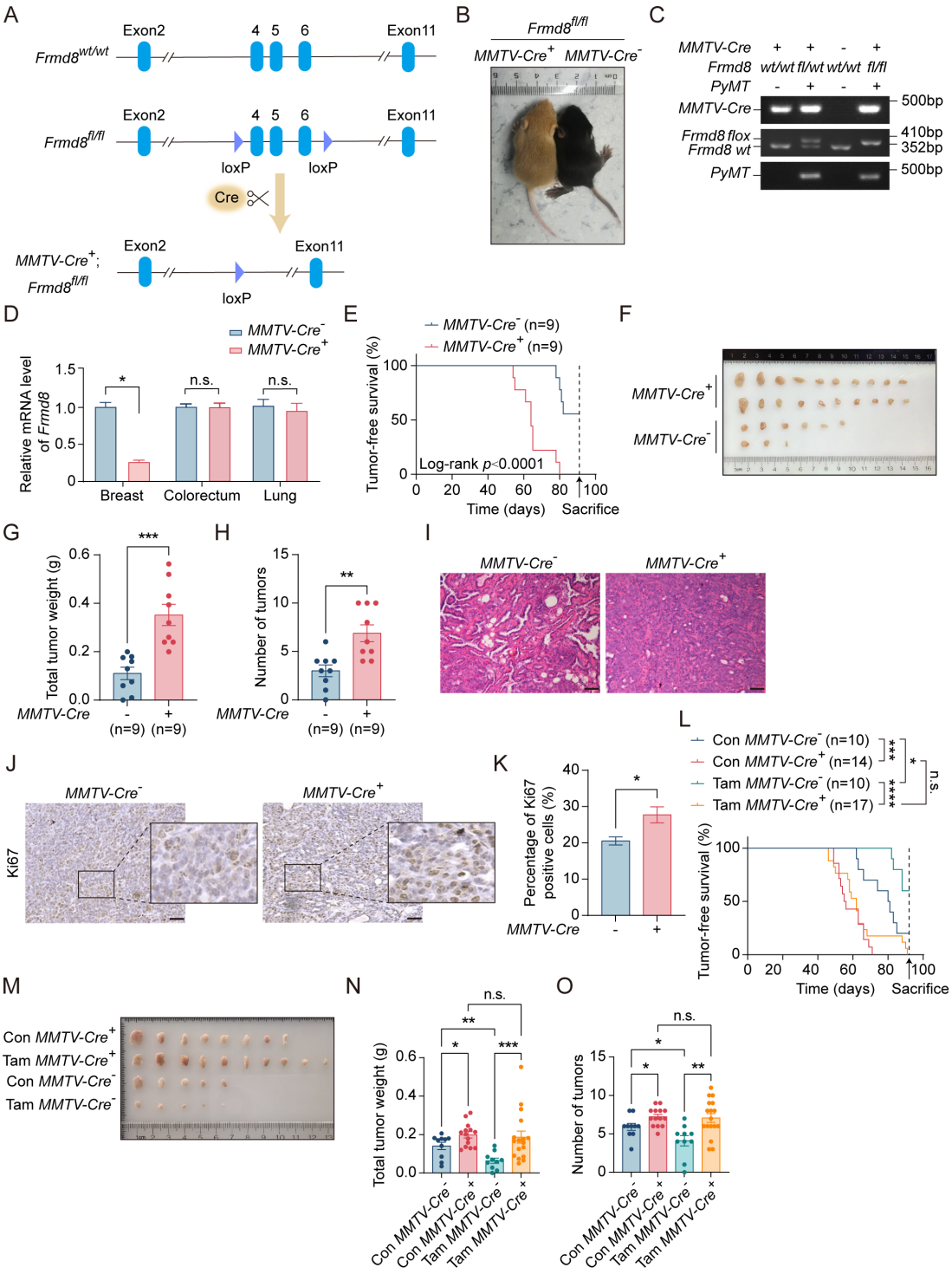

Figure 1. Loss of Frmd8 promotes mammary tumor growth and generates tamoxifen resistance *in vivo*

(A) A diagram of the *Frmd8* targeted alleles. Exons 4, 5 and 6 are flanked by loxp sites. (B) Distinguishing the genotype of littermate mice by mice coat color. Yellow represents *MMTV-Cre*$^{+}$; *Frmd8*$^{fl/fl}$; *PyMT* genotype and black represents *MMTV-Cre*$^{-}$; *Frmd8*$^{fl/fl}$; *PyMT* genotype. (C) Representative PCR genotyping of mouse tail DNA. (D) Relative mRNA level of *Frmd8* in 7-week-old mammary glands from *PyMT* mice was analyzed by qRT-PCR. *Gapdh* was used as an internal reference. **p*<0.05 by unpaired Student's t-test. (E) Kaplan-Meier plot showing the appearance of palpable tumors in *MMTV-Cre*$^{-}$; *Frmd8*$^{fl/fl}$; *PyMT* (n=9) and *MMTV-Cre*$^{+}$; *Frmd8*$^{fl/fl}$; *PyMT* (n=9) mice (Log-rank test). (F) Representative images of tumors from *MMTV-Cre*$^{-}$; *Frmd8*$^{fl/fl}$; *PyMT* and *MMTV-Cre*$^{+}$; *Frmd8*$^{fl/fl}$; *PyMT* mice. (G-H) Total tumor weight (G) and number of tumors (H) per mice were measured. ***p*<0.01, ****p*<0.001 by unpaired Student's t-test. (I) Representative H&E staining of tumors from *MMTV-Cre*$^{-}$; *Frmd8*$^{fl/fl}$; *PyMT* and *MMTV-Cre*$^{+}$; *Frmd8*$^{fl/fl}$; *PyMT* mice. Scale bar, 50 μm. (J) Immunohistochemistry (IHC) staining for Ki67 expression in mammary tumors from *PyMT* mice. The black boxes represent the magnified typical staining of the original images. Scale bar, 50 μm. (K) Quantification of Ki67-positive cell percentage in (J). **p*<0.05 by unpaired Student's t-test. (L) Kaplan-Meier plot showing the appearance of palpable tumors in *MMTV-Cre*$^{-}$; *Frmd8*$^{fl/fl}$; *PyMT* and *MMTV-Cre*$^{+}$; *Frmd8*$^{fl/fl}$; *PyMT* mice, with or without tamoxifen treatment (Log-rank test, **p*<0.05, ****p*<0.001, *****p*<0.0001). (M) Representative images of tumors from *MMTV-Cre*$^{-}$; *Frmd8*$^{fl/fl}$; *PyMT* and *MMTV-Cre*$^{+}$; *Frmd8*$^{fl/fl}$; *PyMT* mice, with or without tamoxifen treatment. (N-O) Total tumor weight (N) and number of tumors (O) per mice from (L) were measured. **p*<0.05, ***p*<0.01, ****p*<0.001 by unpaired Student's t-test or Mann Whitney test.

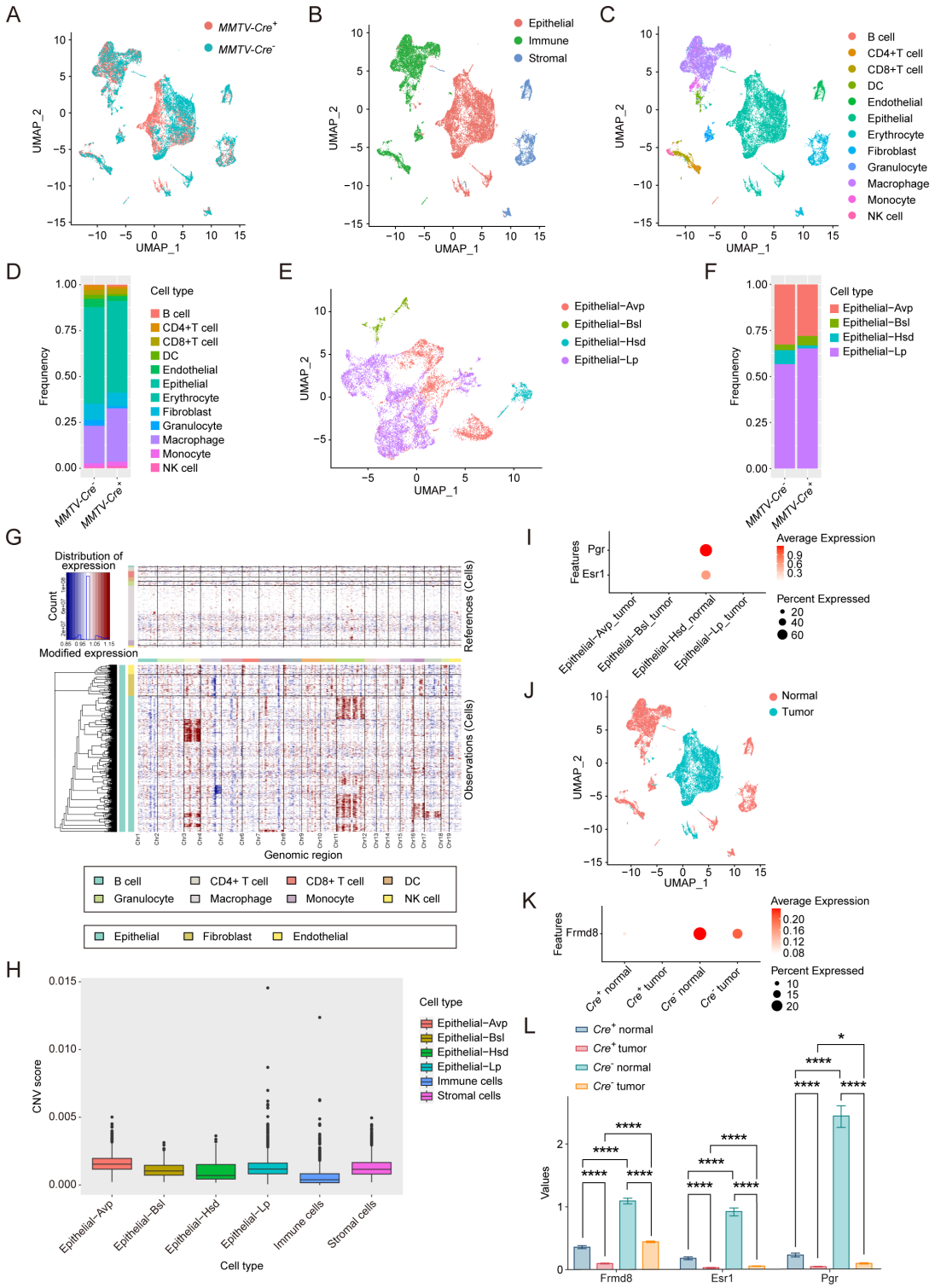

Figure 2. Frmd8 knockout decreases the proportion of the hormone-sensing differentiated epithelial cells

(A) T-SNE plot showing the distribution of cells from *MMTV-Cre*$^{-}$; *Frmd8*$^{fl/fl}$; *PyMT* and *MMTV-Cre*$^{+}$; *Frmd8*$^{fl/fl}$; *PyMT* mice. (B) T-SNE plot showing the distribution of

epithelial, immune and stromal cells. (C-D) T-SNE plot showing the distribution of main cell linages (C) and their relative percentage (D). (E-F) T-SNE plot showing the distribution of epithelial cell linages (E) and their relative percentage (F). (G) Heatmap showing distinct features of each cell lineages. Rows, genes. Columns, cells. The color key from blue to red indicates low to high gene expression. (H) Boxplot showing CNV score of main cell linages. (I) Dot plot showing the expression of *Esr1* and *Pgr* in epithelial cell linages. (J) T-SNE plot showing the distribution of normal cells and tumor cells. (K) Dot plot showing the expression of *Frmd8* in normal and tumor cells from *MMTV-Cre*$^{-}$; *Frmd8*$^{fl/fl}$; *PyMT* and *MMTV-Cre*$^{+}$; *Frmd8*$^{fl/fl}$; *PyMT* mice. (L) Statistical analysis of *Frmd8*, *Esr1* and *Pgr* expression in normal and tumor cells from *MMTV-Cre*$^{-}$; *Frmd8*$^{fl/fl}$; *PyMT* and *MMTV-Cre*$^{+}$; *Frmd8*$^{fl/fl}$; *PyMT* mice. *p<0.05, ****p<0.0001 by Mann-Whitney test.

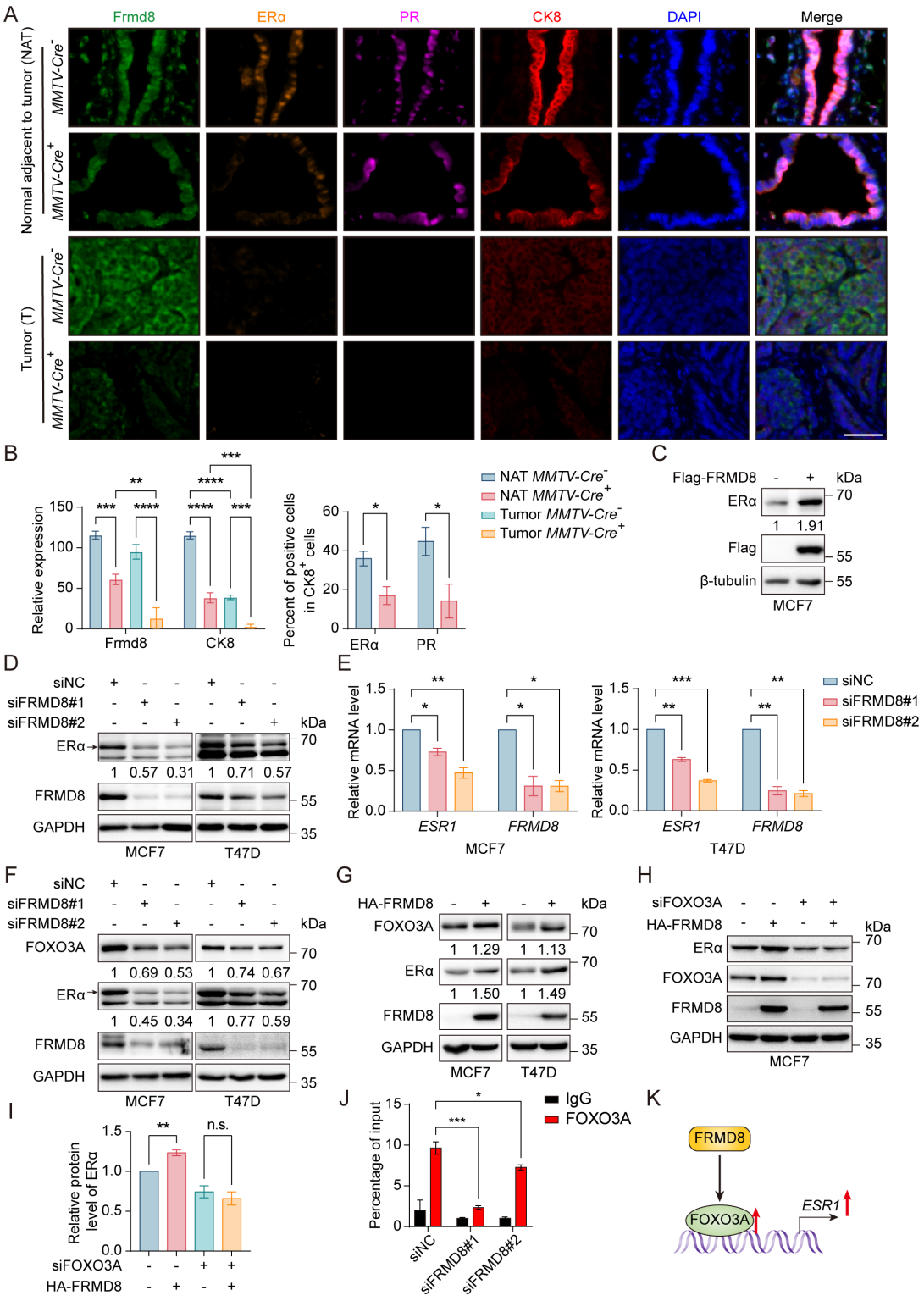

Figure 3. FRMD8 promotion of *ESR1* expression is mediated by FOXO3A

(A) Representative multiplex immunofluorescence images of tumor tissues and tissues adjacent to tumor from *MMTV-Cre*$^{-}$; *Frmd8*$^{fl/fl}$; *PyMT* and *MMTV-Cre*$^{+}$; *Frmd8*$^{fl/fl}$; *PyMT* mice. Scale bar, 50 μm. (B) Qualification of Frmd8 and CK8 expression (left

panel) and ERα and PR-positive cell percentage in $CK8^+$ cells (right panel) in (A). *p<0.05, **p<0.01, ***p<0.001, ****p<0.0001 by one-way ANOVA (left panel) or unpaired Student's t-test (right panel). (C) Lysates from MCF7 cells transiently transfected with Flag or Flag-FRMD8 were immunoblotted. (D) Lysates from MCF7 and T47D cells transiently transfected with control or FRMD8 siRNA were immunoblotted. In this and subsequent figures, specific bands are marked with an arrow. (E) Relative mRNA levels of *ESR1* and *FRMD8* from MCF7 and T47D cells transiently transfected with control or FRMD8 siRNA were analyzed by qRT-PCR. *GAPDH* was used as an internal reference. *p<0.05, **p<0.01, ***p<0.001 by one-way ANOVA. (F) Lysates from MCF7 and T47D cells transiently transfected with control or FRMD8 siRNA were immunoblotted. (G) Lysates from MCF7 and T47D cells transiently transfected with HA or HA-FRMD8 were immunoblotted. (H-I) Lysates of MCF7 cells co-transfected with HA-FRMD8 and FOXO3A siRNA as indicated were immunoblotted (H). ERα protein levels were quantified by normalizing to the intensity of the GAPDH band (I). **p<0.01 by unpaired Student's t-test. (J) Lysates of T47D cells transfected with control or FRMD8 siRNA were subjected to anti-FOXO3A ChIP-qPCR. *p<0.05, ***p<0.001 by one-way ANOVA. (K)Working model for FRMD8 promotes *ESR1* transcription via upregulating FOXO3A expression.

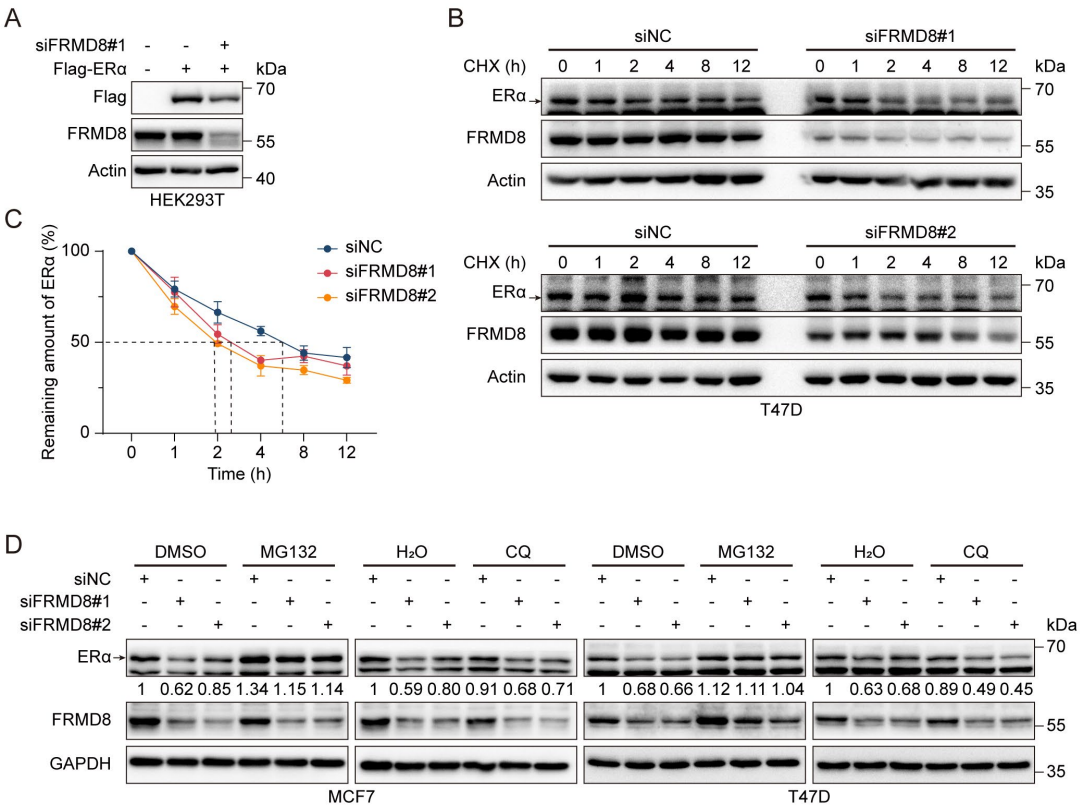

827

828 **Figure 4. FRMD8 stabilizes ERα via prevention of its degradation**

829 (A) Lysates of HEK293T cells co-transfected with Flag-ERα and FRMD8 siRNA as
830 indicated were immunoblotted. (B-C) Lysates from T47D cells transiently transfected
831 with control or FRMD8 siRNA were subjected to immunoblotting. Cells were treated
832 with 100 μg/ml CHX for the indicated times (B). ERα protein levels were quantified by
833 normalizing to the intensity of the Actin band (C). (D) Immunoblot analysis of ERα in
834 MCF7 (D) and T47D (E) cells transiently transfected with control or FRMD8 siRNA.
835 The cells were treated with MG132 (25 μM) or chloroquine (50 μM) for 6 h.

836

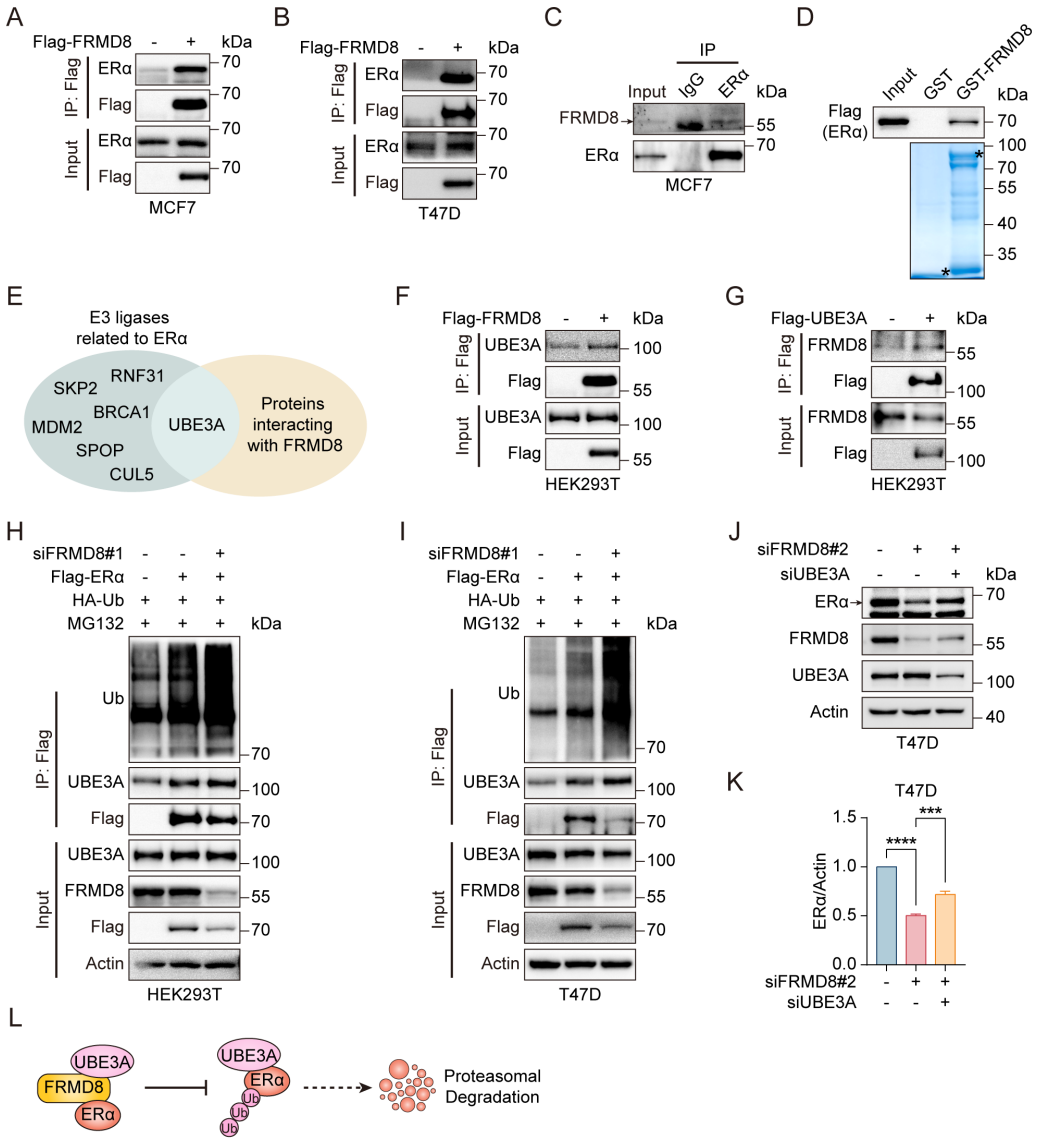

Figure 5. FRMD8 inhibits ERα degradation by blocking UBE3A binding with ERα

(A-B) Lysates of MCF7 (A) and T47D (B) cells transfected with Flag or Flag-FRMD8 were anti-Flag immunoprecipitated and immunoblotted for ERα and Flag. (C) Lysates from MCF7 cells were immunoprecipitated with IgG or anti-ERα, then immunoblotted for FRMD8 and ERα. (D) HEK293T cells were transiently transfected with Flag-ERα. ERα proteins in HEK293T whole cell lysates (WCL) pulled down by GST or GST-FRMD8 recombinant proteins were subjected to Western blot. Asterisks indicate proteins at the expected molecular weight. (E) Venn diagram showing overlap of E3 ligases related to ERα and proteins interacting with FRMD8. (F) Lysates of HEK293T cells transfected with Flag or Flag-FRMD8 were anti-Flag immunoprecipitated and

immunoblotted. (G) Lysates of HEK293T cells transfected with Flag or Flag-UBE3A were anti-Flag immunoprecipitated and immunoblotted. (H-I) HEK293T (H) and T47D (I) cells were co-transfected with Flag-ERα, HA-Ub and FRMD8 siRNA as indicated. Cells were treated with MG132 (25 μM) for 6 h. WCL were immunoprecipitated with anti-Flag and then immunoblotted for ubiquitinated ERα. (J-K) Lysates of T47D cells co-transfected with FRMD8 and UBE3A siRNA as indicated were immunoblotted (J). ERα protein levels were quantified by normalizing to the intensity of the Actin band (K). ***$p<0.001$, ****$p<0.0001$ by one-way ANOVA. (L) Working model for FRMD8 disrupts the interaction between ERα and UBE3A, and protects ERα from UBE3A-mediated degradation.

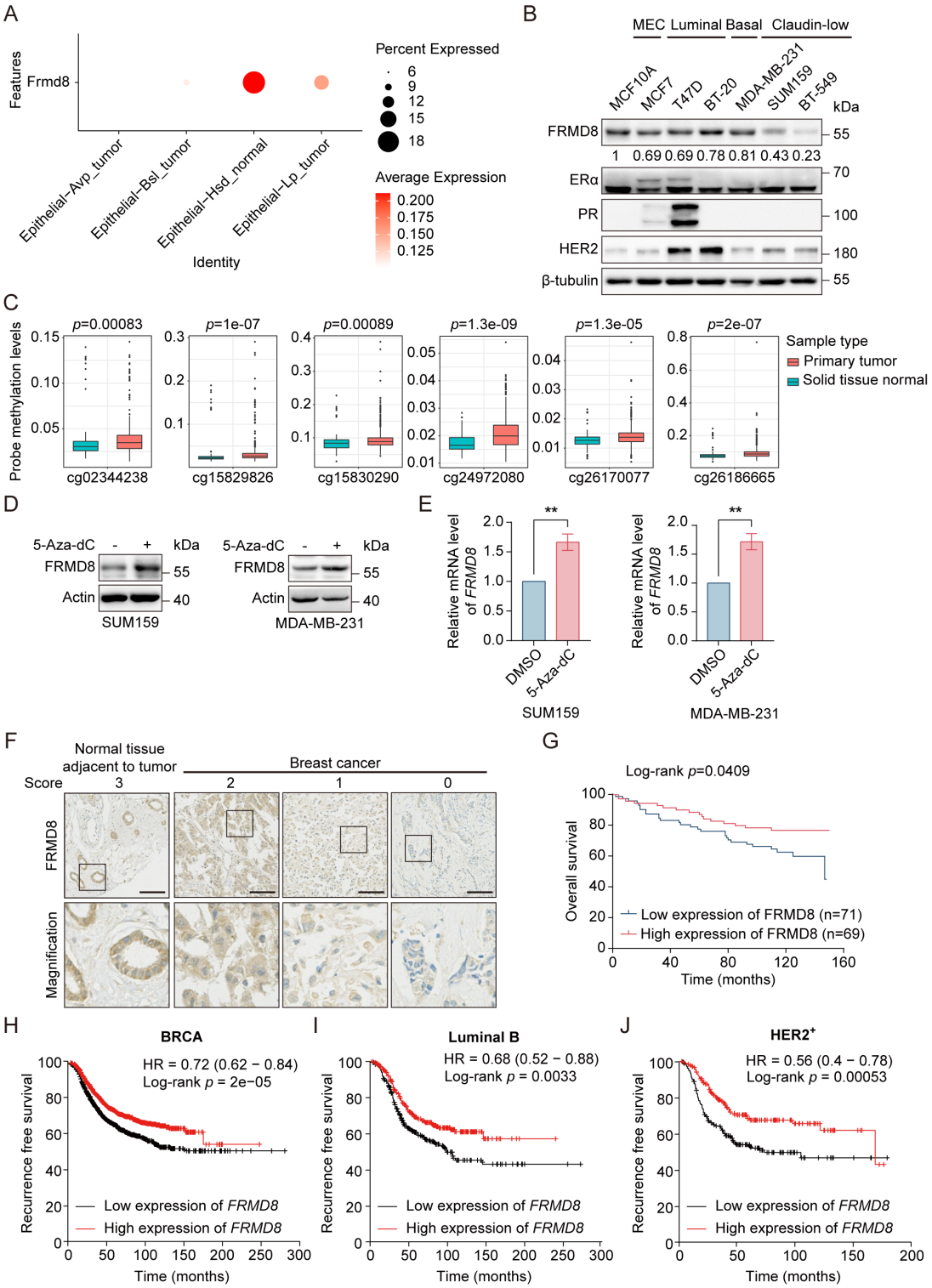

Figure 6. *FRMD8* promoter is methylated and low FRMD8 level predicts poor prognosis in breast cancer patients

(A) Dot plot showing the expression of *Frmd8* in epithelial cell linages from *PyMT* mice. (B) Lysates from human mammary epithelial cell (MEC) and breast cancer cells

were subjected to immunoblotting. (C) Methylation of *FRMD8* promoter region in breast cancer according to the University of California Santa Cruz (UCSC) database (http://xena.ucsc.edu/). (D) SUM159 and MDA-MB-231 cells were treated with 5-Aza-dC (10 μM) for 48 h. Protein expression of FRMD8 was examined by Western blot. (E) SUM159 and MDA-MB-231 cells were treated with 5-Aza-dC (10 μM) for 48 h. *FRMD8* mRNA levels was examined by quantitative reverse transcription PCR (qRT-PCR) *GAPDH* was used as an internal reference. $^{**}p<0.01$ by unpaired Student's t-test. (F) IHC analysis of FRMD8 expression in human breast carcinoma TMA was performed. Representative examples (scale bar, 100 μm) of normal tissue adjacent to tumor and breast cancer with different levels of FRMD8 expression are shown, with the magnification of selected areas inserted. (G) Kaplan-Meier analysis for the overall survival of breast cancer patients according to FRMD8 expression (Log-rank test). (H-J) Recurrence free survival of breast cancer patients according to *FRMD8* expression were analyzed according to Kaplan-Meier plotter (http://kmplot.com/analysis/).

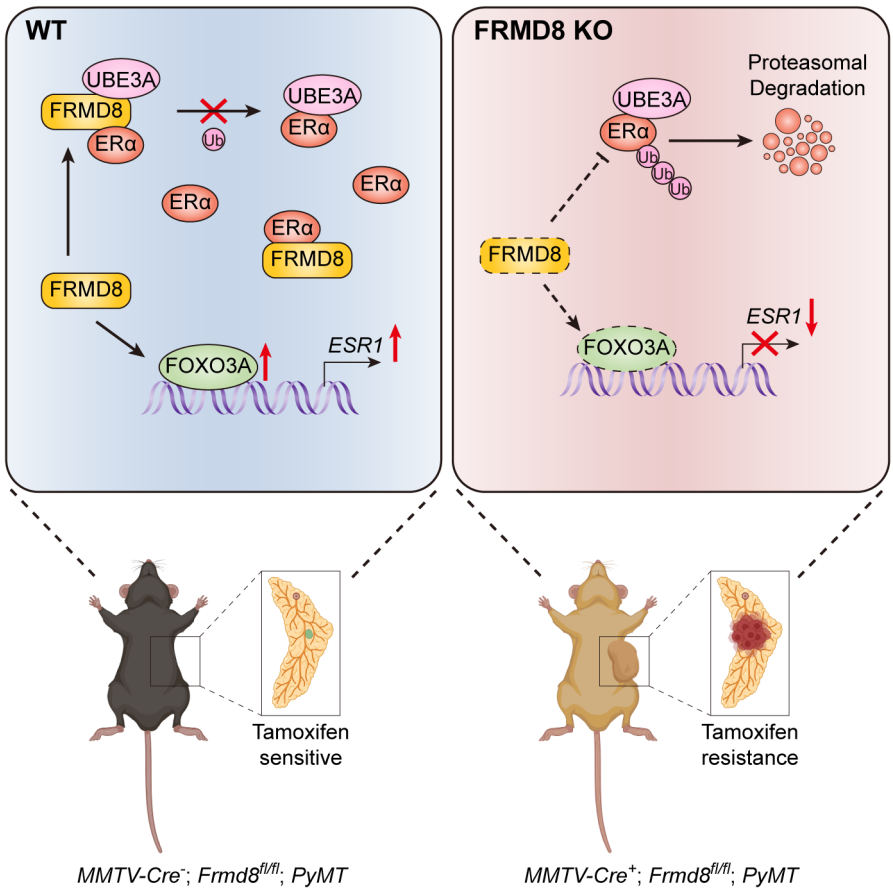

879

880 **Figure 7. A working model shows that loss of FRMD8 promotes mammary tumor**
881 **progression and confers tamoxifen resistance by downregulating ERα expression**
882 **at both transcriptional and post-translational levels.**